Support Information

Effect of Alkylthiophene Spacers and Fluorination on the Optoelectronic Properties of 5,10-Bis(alkylthien-2-yl)dithieno[2,3-*d*:2′,3′-*d*′]benzo[1,2-*b*:4,5-*b*′]dithiophene-*alt*-benzothiadiazole Derivatives Copolymers

Pengzhi Guo,[a] Jingbiao Sun,[a] Shuo Sun,[b] Jianfeng Li,[a] Junfeng Tong,[b] Chuang Zhao,[b] Liangjian Zhu,[a] Peng Zhang,[a] Chunyan Yang,[a] Yangjun Xia [a,c,]

[a.]Key Lab of Optoelectronic Technology and Intelligent Control of Education Ministry, Lanzhou Jiaotong University, Gansu Province, Lanzhou, 730070, China.

[b.]National Laboratory for Infrared Physics, Shanghai Institute of Technical Physics, Chinese Academy of Sciences, Shanghai 200083, China

[c.] Centre for Polymers and Organic Solids, University of California, Santa Barbara, CA 93106-9510

Contents

1. Thermogravimetric characteristics of the copolymers.
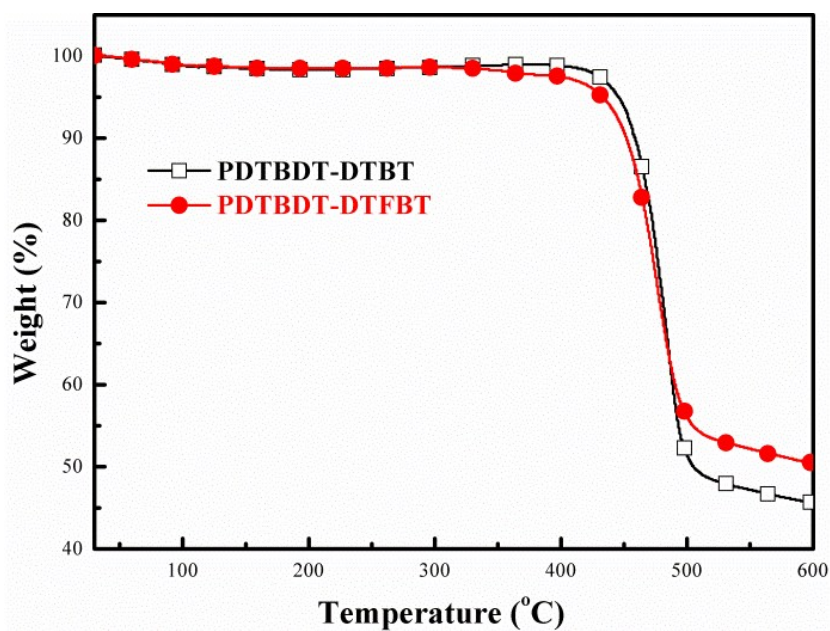
Fig. S1. Thermogravimetric curves of the copolymers.

2. Normalized absorption of the PDTBDT-BT and PDTBDT-FBT.
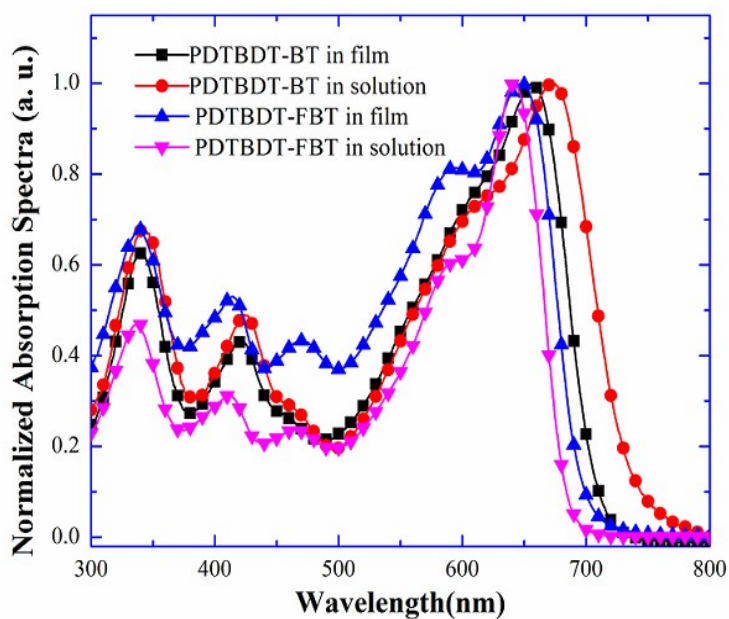
Fig. S2. Normalized absorption of PDTBDT-BT and PDTBDT-FBT in dilute solution and film.

3. Temperature-dependant photoluminescence spectra of the PDTBDT-DTBT and PDTBDT-DTFBT in dilute solution.

Fig. S3. Normalized temperature-dependent photoluminescence spectra of PDTBDT-DTBT (a) and PDTBDT-DTFBT (b) in dilute solution.

4. Temperature-dependant absorption spectra of the PDTBDT-DTBT and PDTBDT-DTFBT in film.

Fig. S4. Normalized temperature-dependent UV−vis spectra of PDTBDT-DTBT (a) and PDTBDT-DTFBT in solid states.

5. Temperature-dependant photoluminescence spectra of the PDTBDT-DTBT and PDTBDT-DTBT and PDTBDT-DTFBT in films.
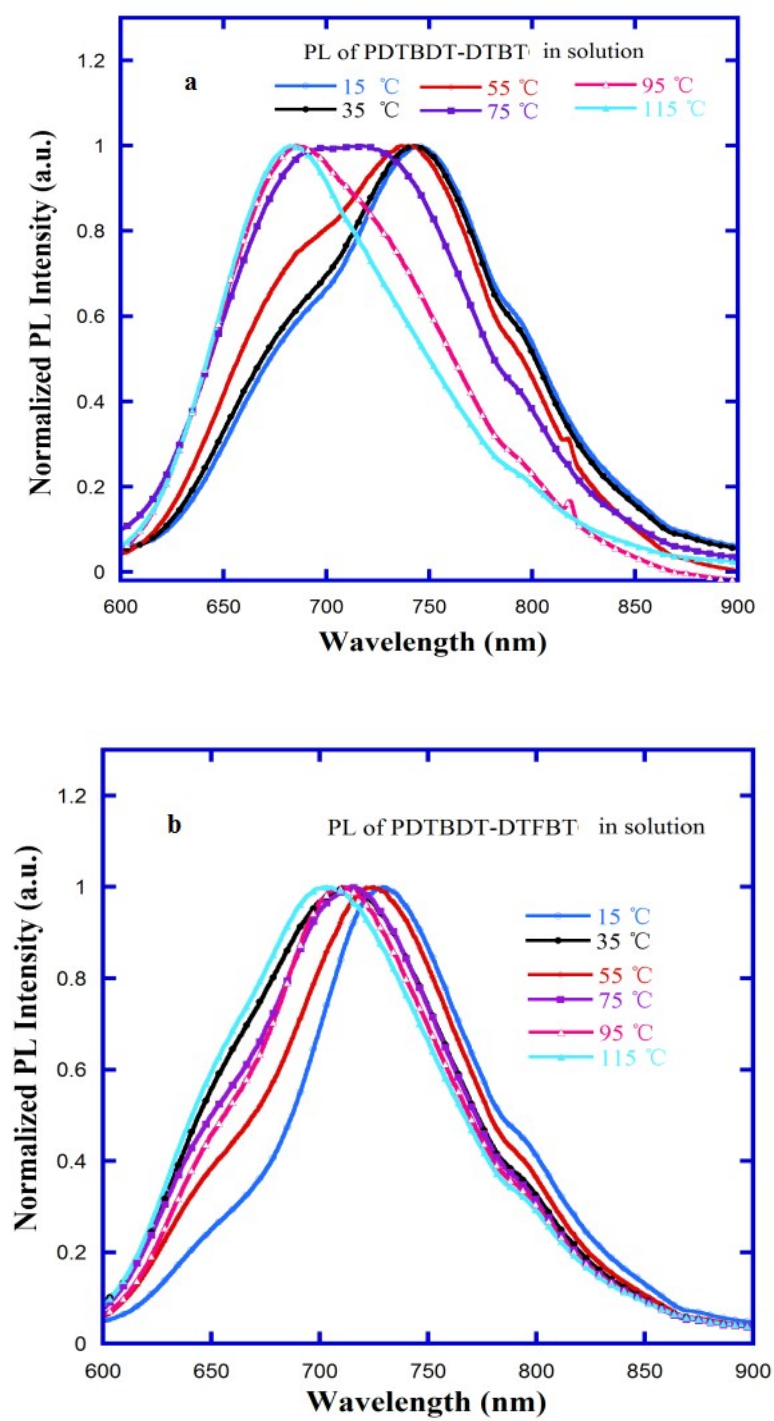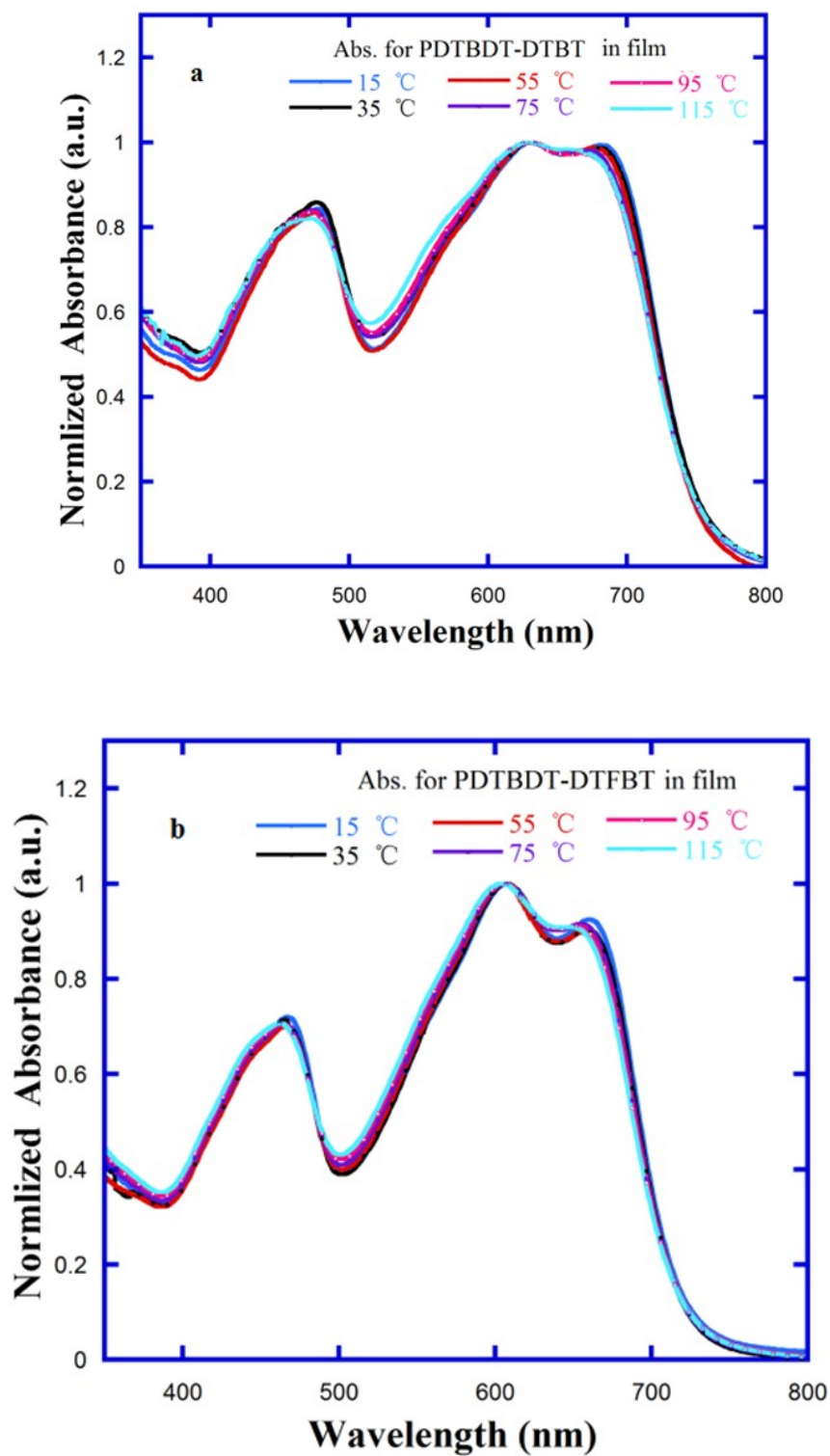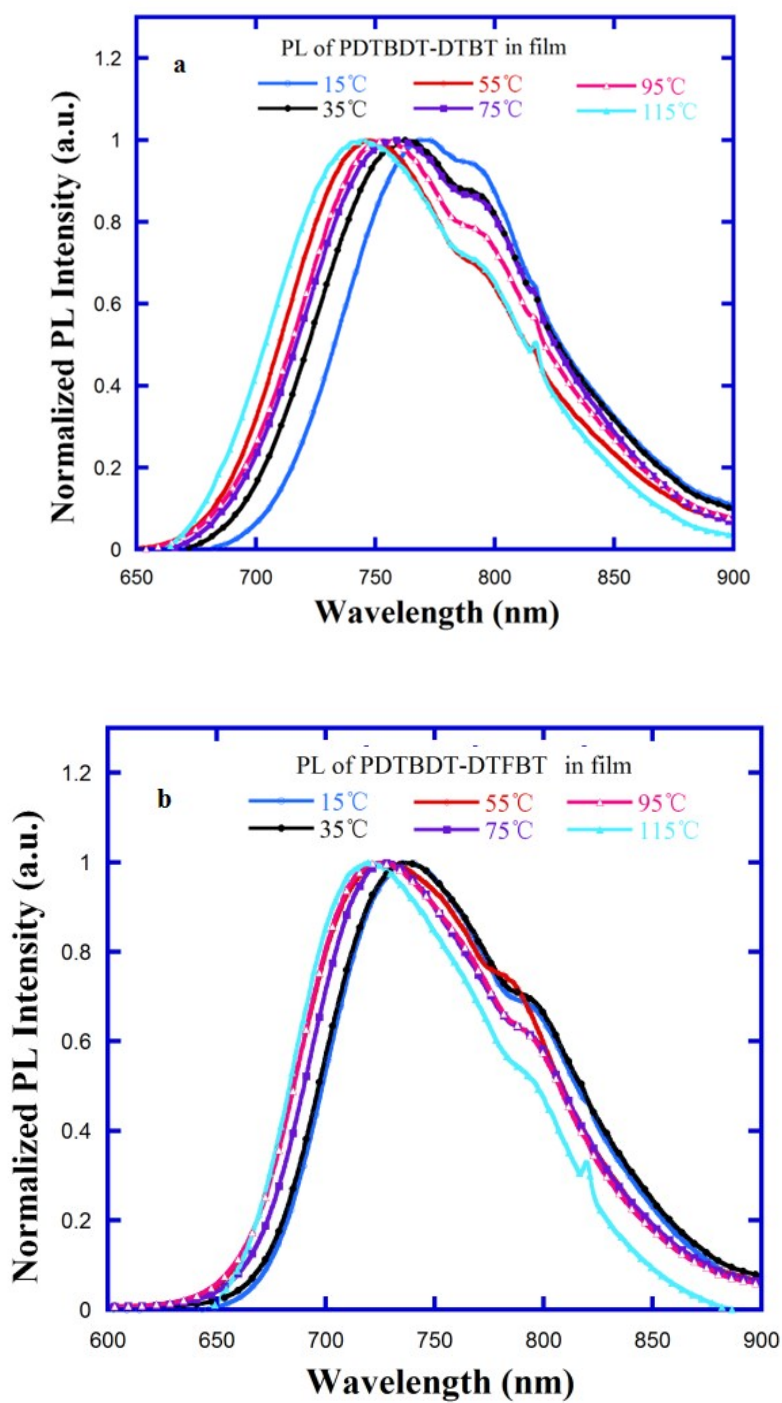

Fig. S5. Normalized temperature-dependent photoluminescence spectra of PDTBDT-DTBT (a) and PDTBDT-DTFBT (b) in solid states.

6. Temperature-dependant absorption spectra of the PDTBDT-DTBT (a) and PDTBDT-DTFBT (b) in dilute solution.
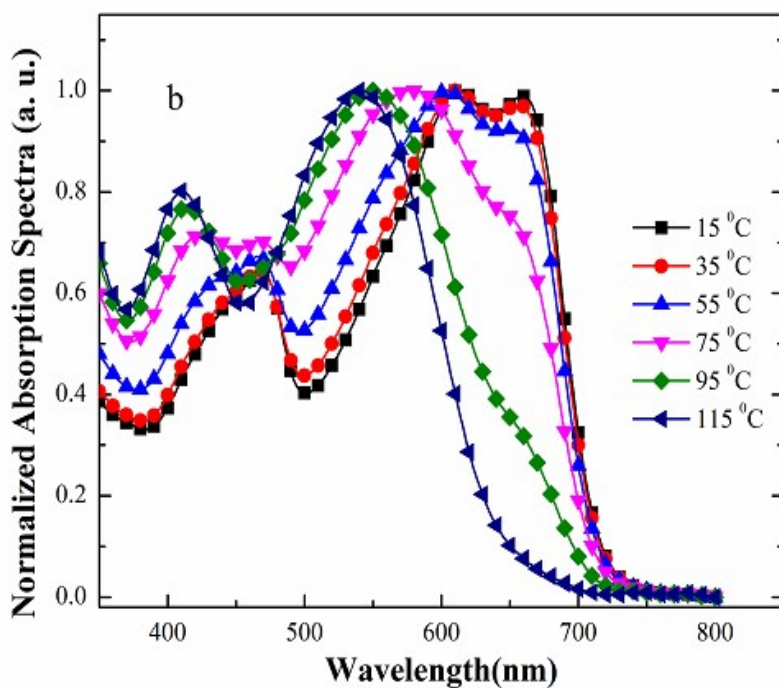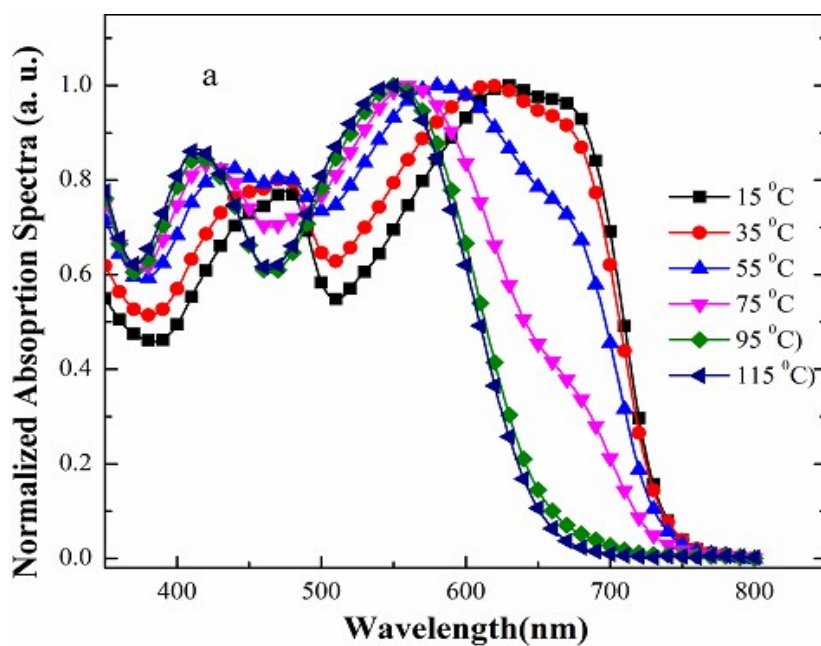
Fig. S6. Temperature-dependent UV−vis spectra of PDTBDT-DTBT (a) and PDTBDT-DTFBT (b) in chlorobenzene solution.

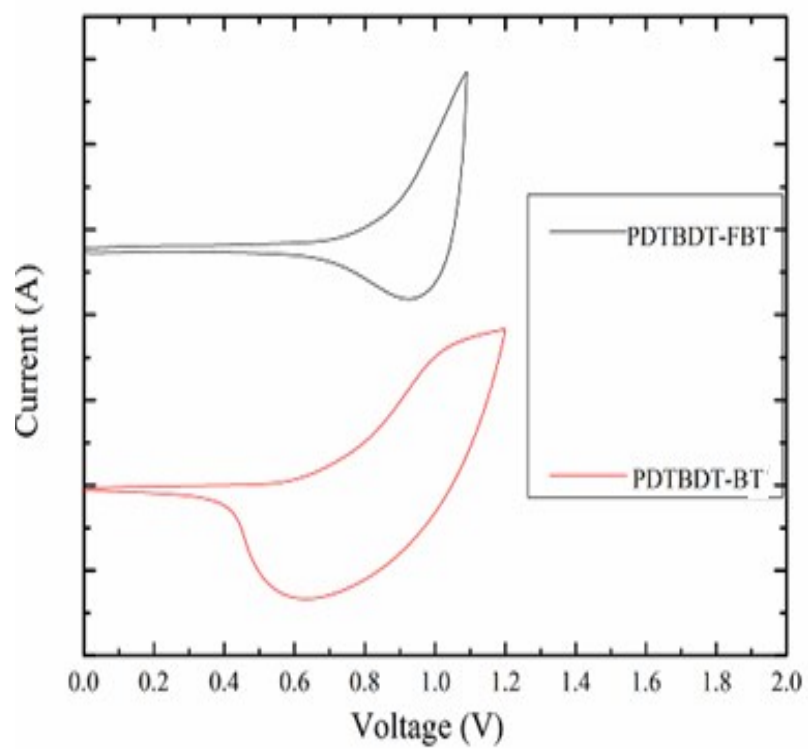7. Electrochemical characteristics of the PDTBDT-BT and PDTBT-FBT.

Fig. S7. Cyclic voltammetry curves of PDTBDT-BT and PDTBDT-FBT measured in a nitrogen-saturated solution of 0.1 M tetrabutylammonium hexafluorophosphate in acetonitrile with glass carbon and Ag/AgNO$_3$ electrodes as the working and reference electrodes, respectively.

8 The method used to calculate the HOMO and LUMO levels for the polymers

Electrochemical cyclic voltammetry measurements were carried out using a CHI660 electrochemical workstation equipped with a glass carbon working electrode, Ag/AgNO$_3$ electrode as the reference electrode, and a Pt wire counter electrode. The measurements were done in anhydrous acetonitrile with tetrabutylammonium hexafluorophosphate (0.1 M) as the supporting electrolyte under an argon atmosphere at a scan rate of 50 mV/s. The potential of the Ag/AgNO$_3$ reference electrode was internally calibrated using the ferrocene/ferrocenium redox couple (Fc/Fc$^+$), which has a known reduction potential of -4.8 eV. The HOMO and LUMO energy levels were calculated by the following equations. $E_{HOMO} = -(E_{ox} + 4.71)$ (eV) and $| E_{LUMO} = -(E_{red}+4.71)$ (eV), the E$_{1/2}$ of ferrocene/ferrocenium (Fc/Fc$^+$) was observed at 0.09 V vs Ag/Ag$^+$..
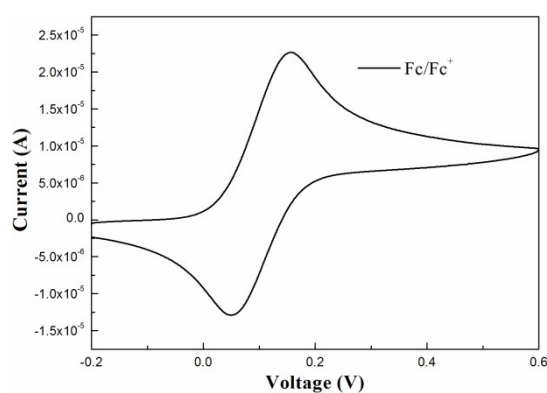

Figure S8. Electrochemical cyclic voltammetry curves of the Fc/Fc$^+$.

9. Optimized geometries of each trimer models (Top view, (a), Side view, (b)) and surface plots and energy levels of frontier orbitals (c) of PDTBDT-DTBT.
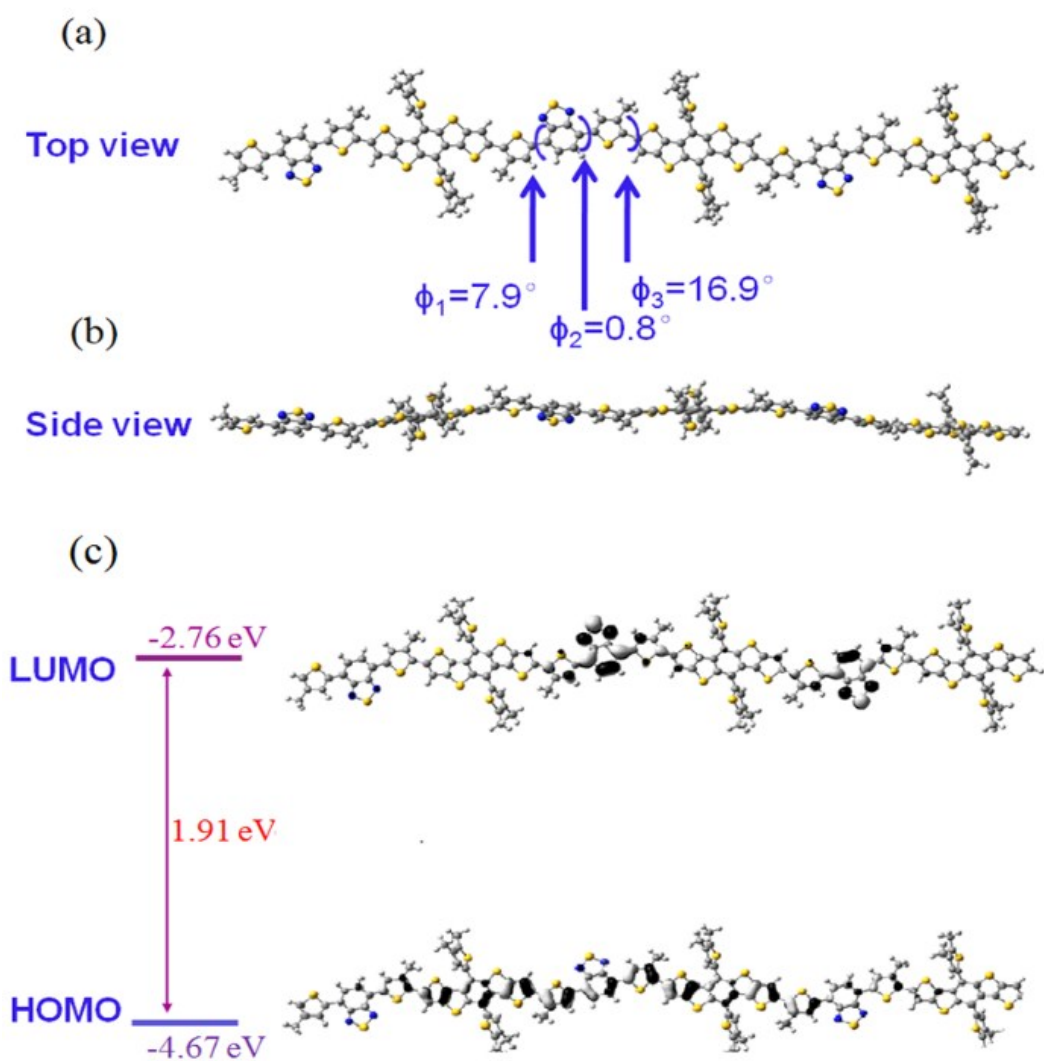

Fig. S9. Optimized geometries of each trimer models (Top view, (a), Side view, (b)) and surface plots and energy levels of frontier orbitals (c) of PDTBDT-DTBT.

10. Optimized geometries of each trimer models (Top view, (a), Side view, (b)) and surface plots and energy levels of frontier orbitals (c) of PDTBDT-DTFBT.
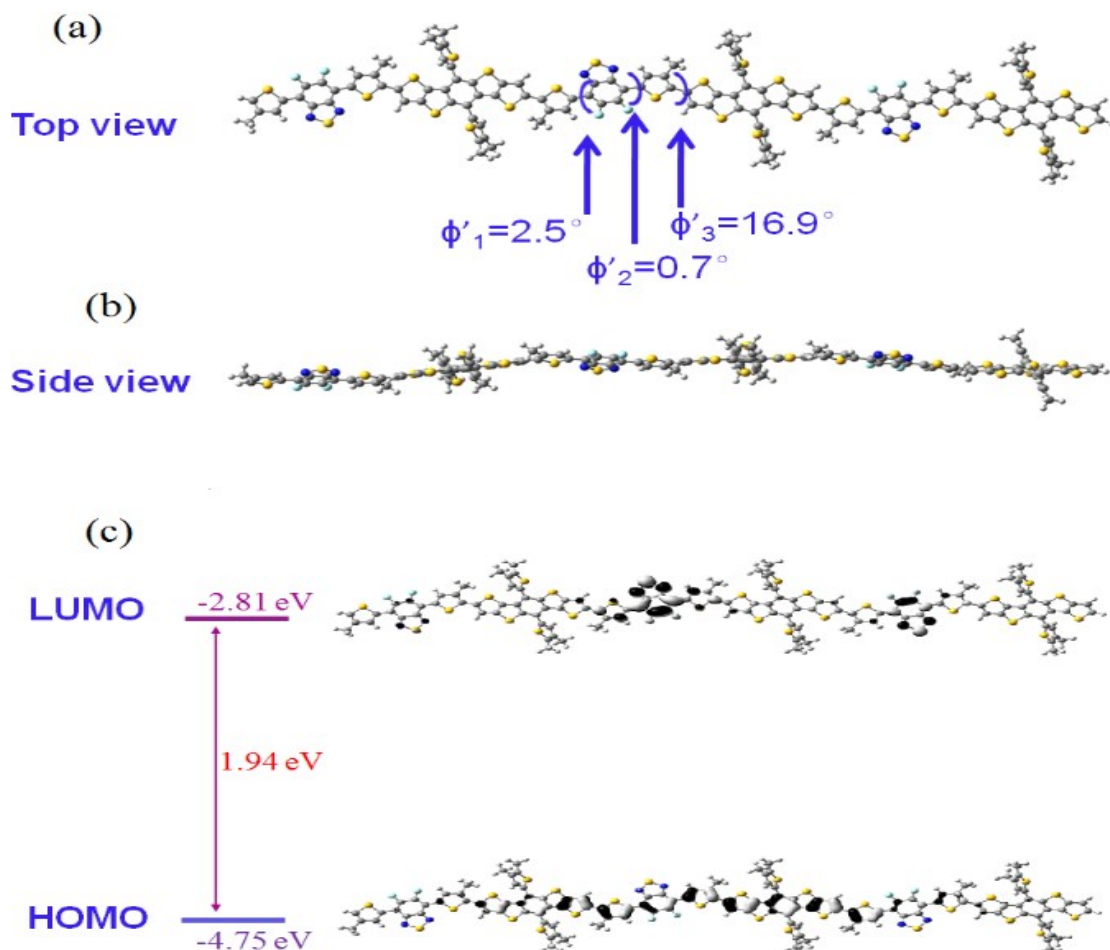

Fig. S10. Optimized geometries of each trimer models (Top view, (a), Side view, (b)) and surface plots and energy levels of frontier orbitals (c) of PDTBDT-DTFBT.

11. Optimized geometries of each trimer models and surface plots (a) and energy levels of frontier orbitals of PDTBDT-BT (b).
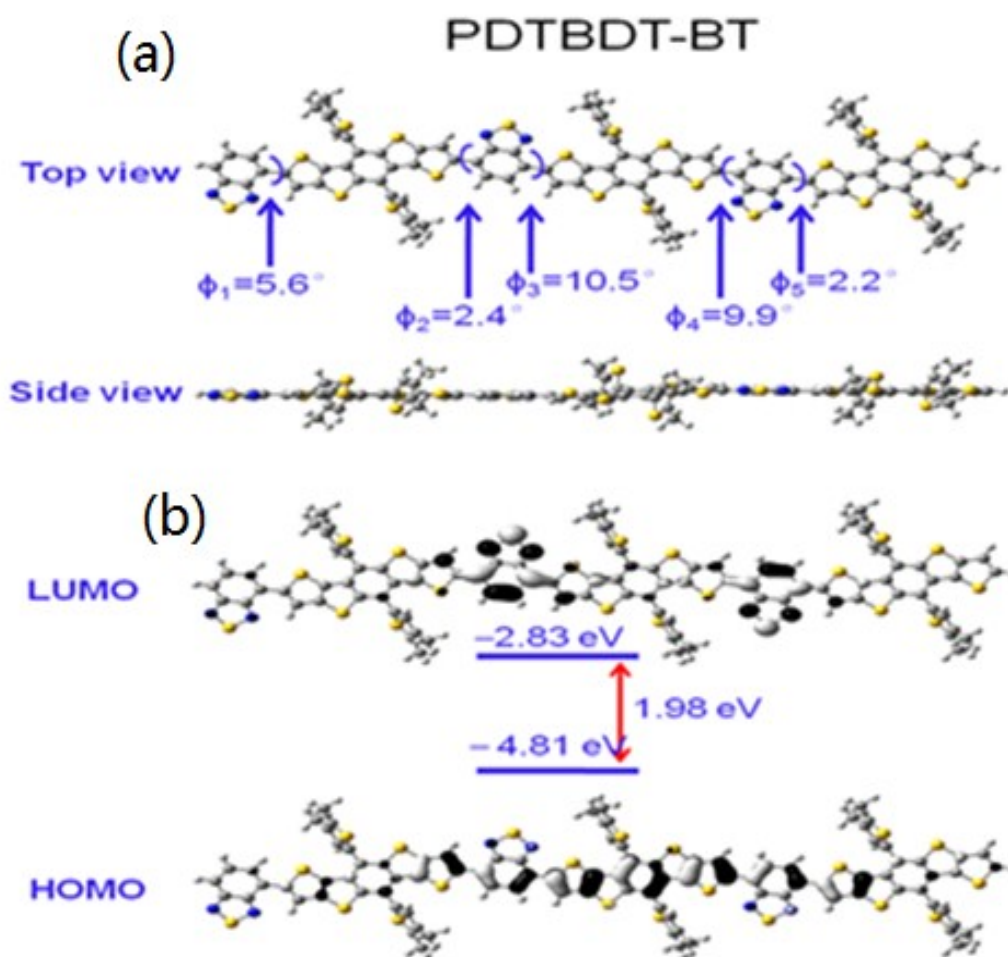

Fig. S11. Optimized geometries of each trimer models and surface plots (a) and energy levels of frontier orbitals of PDTBDT-BT (b).

12. Optimized geometries of each trimer models and surface plots (a) and energy levels of frontier orbitals of PDTBDT-BT (b).
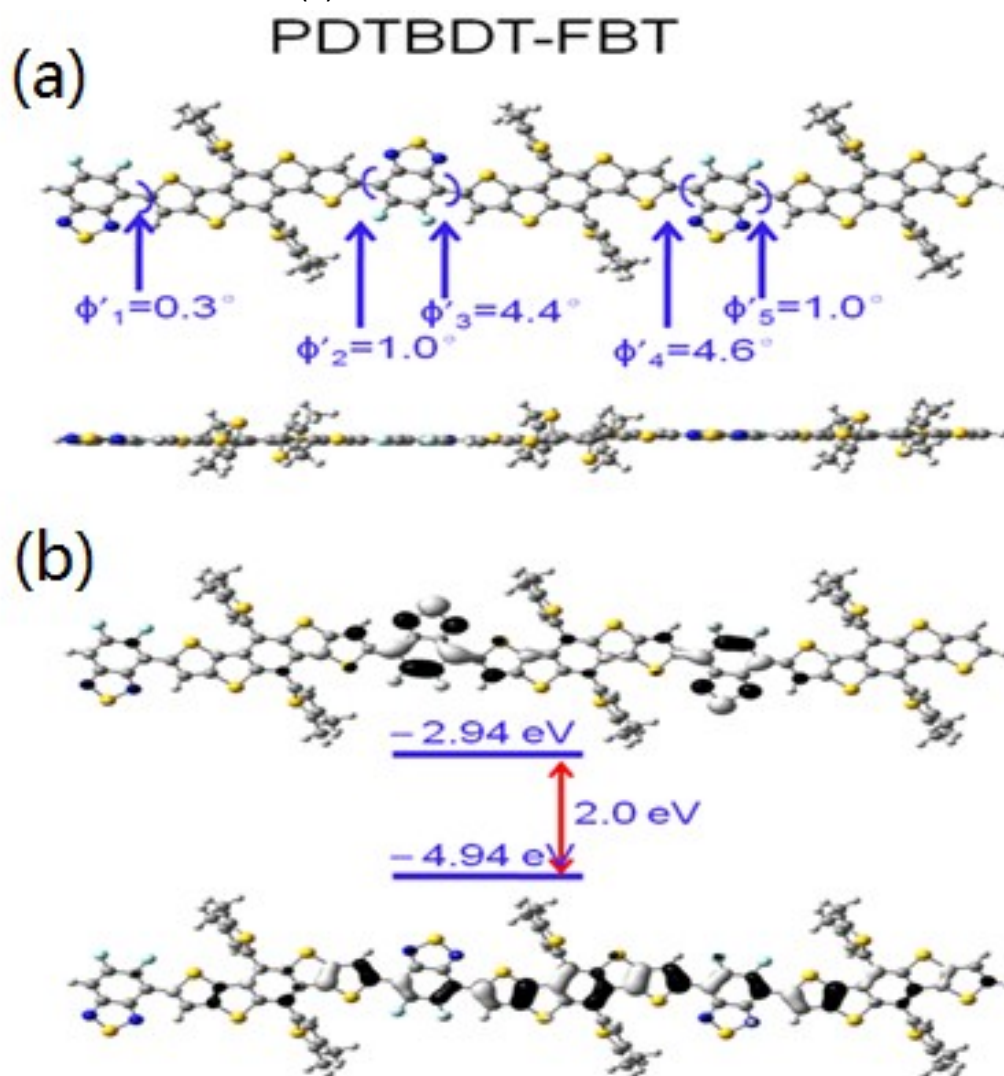

Figure S12. Optimized geometries of each trimer models (a) and surface plots and energy levels of frontier orbitals of PDTBDT-FBT (b).
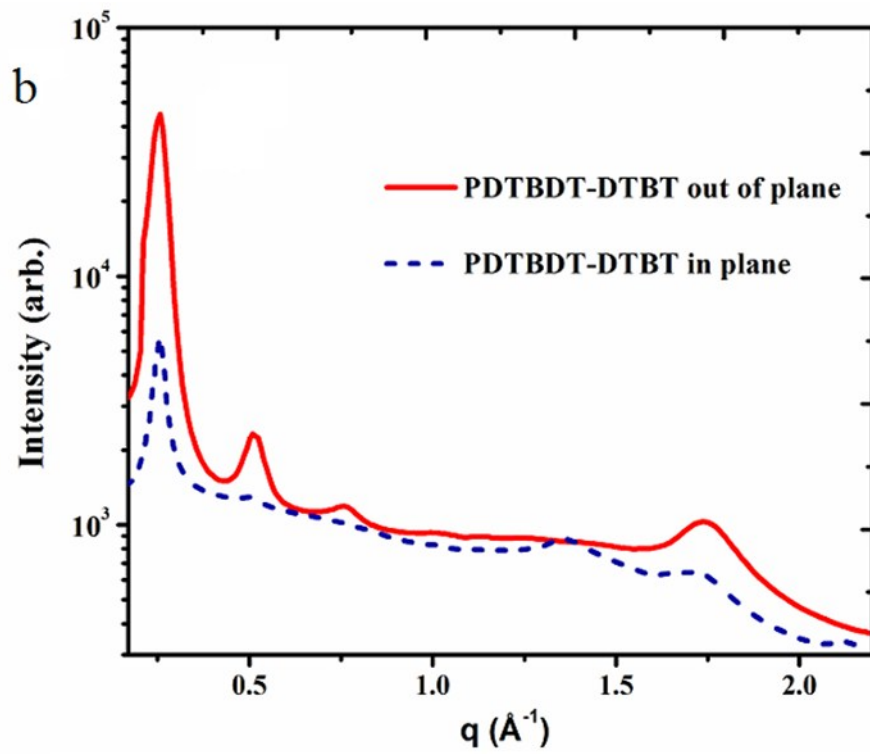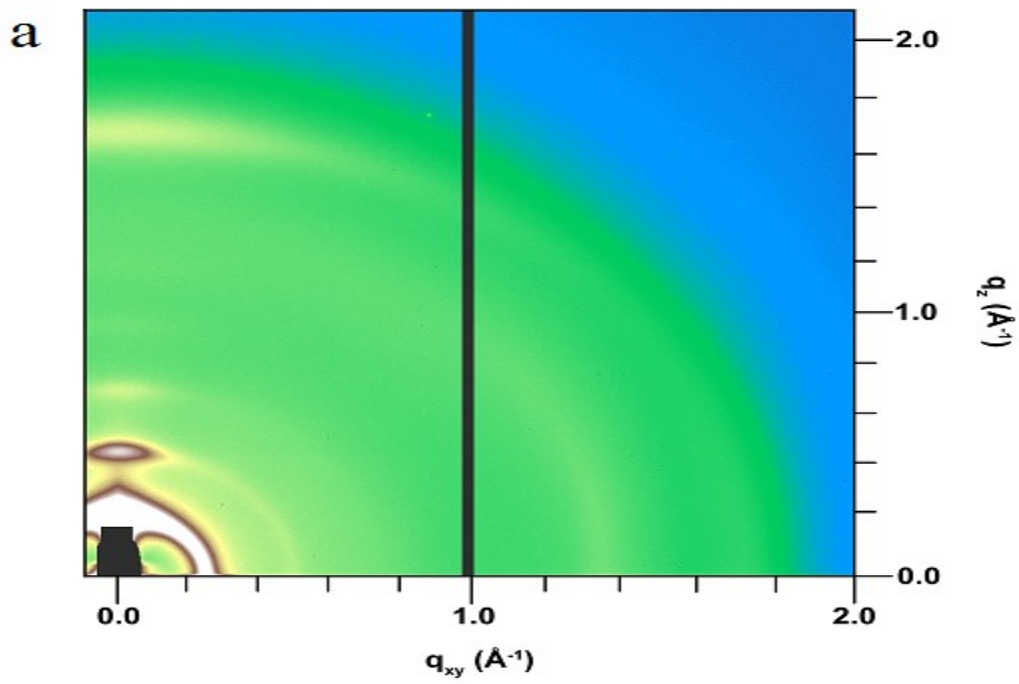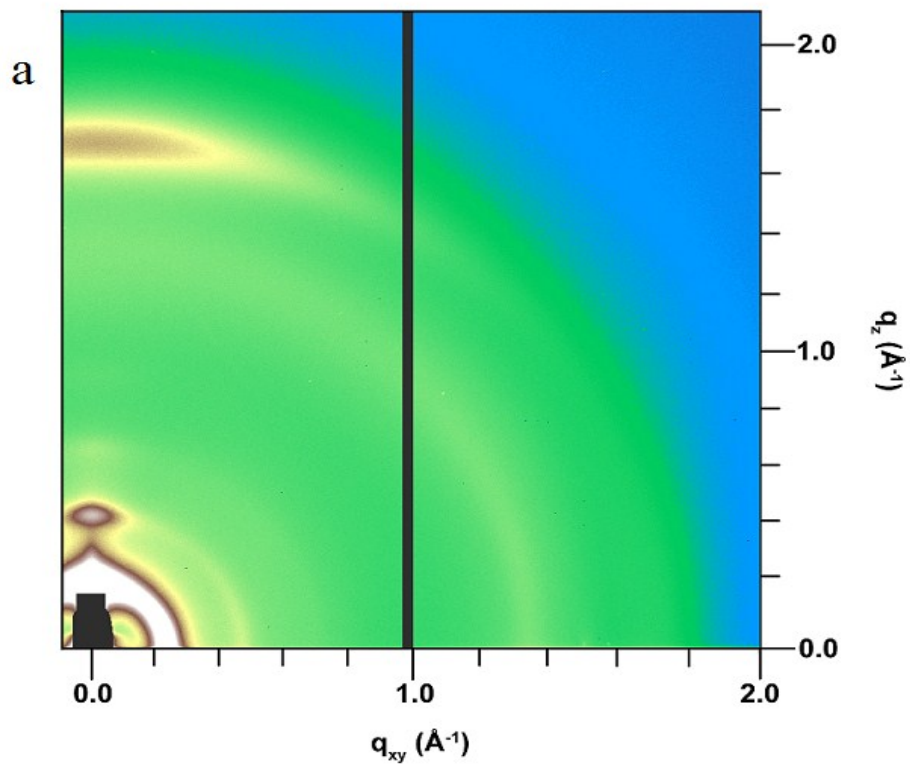
13. 2D-GIWAXs characteristics of the PDTBDT-DTBT

Fig. S13. 2D-GIWAXs patterns and corresponding out-off plane and in-plane line-cut profiles of PDTBDT-DTBT pristine film
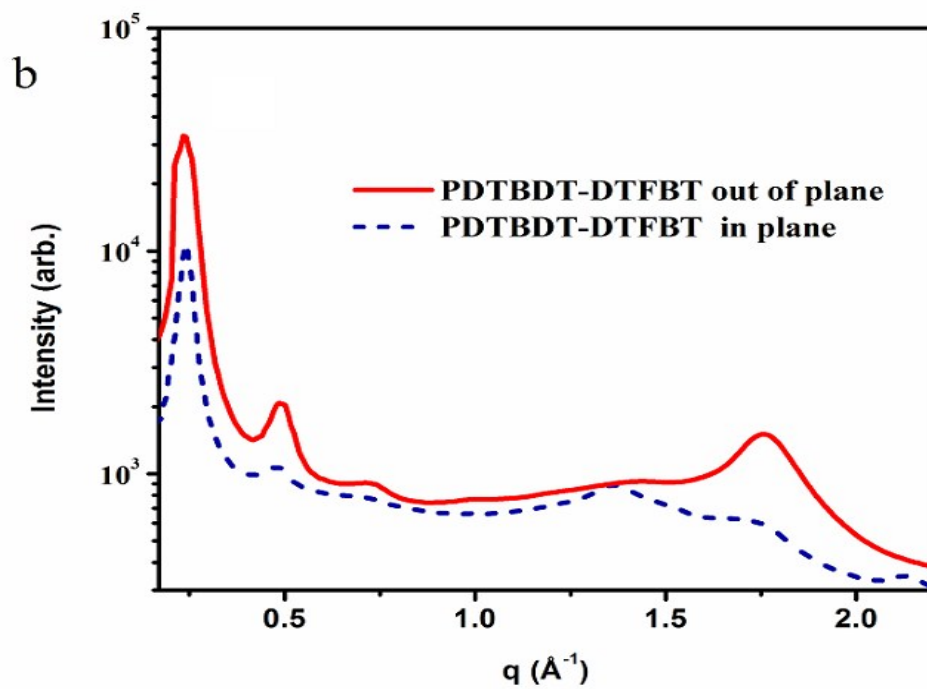
14. 2D GIWAXs characteristics of the PDTBDT-DTBT

Fig. S14. 2D-GIWAXs patterns and corresponding out-off plane and in-plane line-cut profiles of PDTBDT-DTFBT pristine film

15. $J^{0.5}$ –V characteristics of the copolymers in the hole-only devices with configuration of ITO/PEDOT: PSS/copolymers/Au.
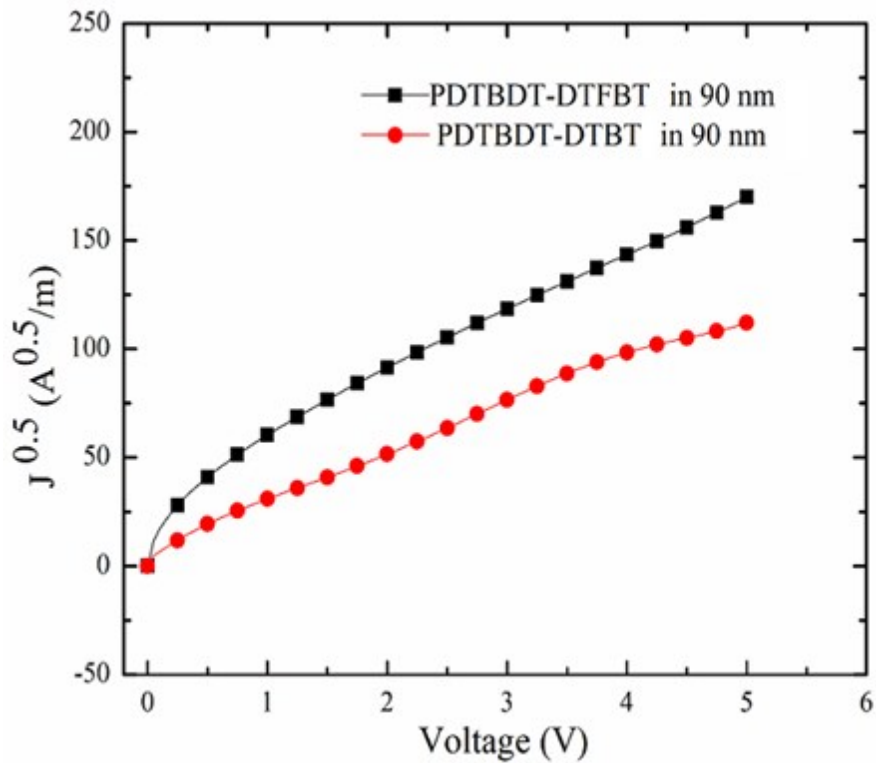

Fig. S15. $J^{0.5}$ –V characteristics of the copolymers in the hole-only devices with configuration of ITO/PEDOT: PSS/copolymers/Au.

16. AFM topography images of the PDTBDT-DTBT/PC$_{71}$BM (a, without DIO, b with 3% DIO) with weight ratio of 1:2.
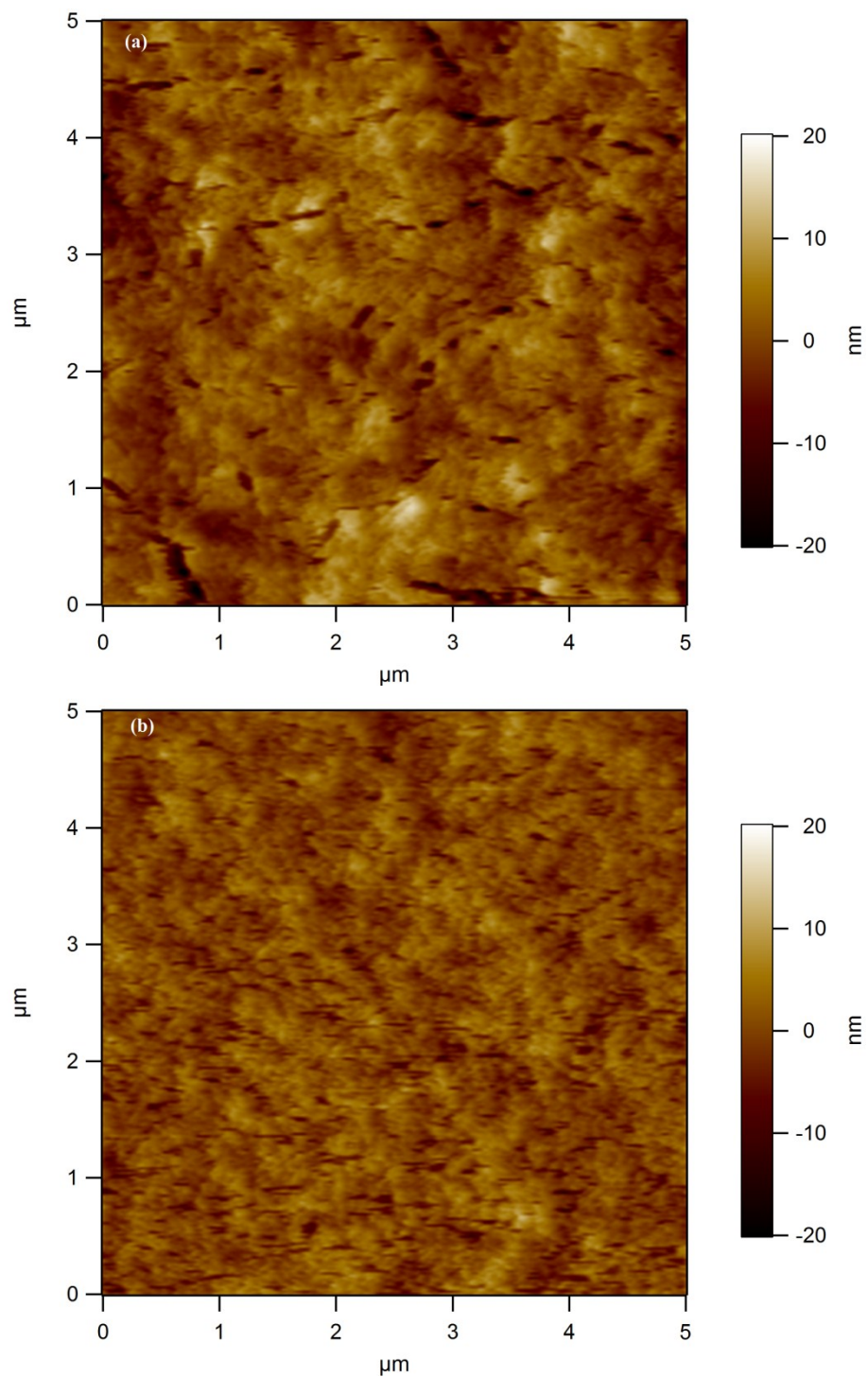

Fig. S16. AFM topography images of the PDTBDT-DTBT/PC$_{71}$BM (a, without DIO, b with 3% DIO) with weight ratio of 1:2.

17. AFM topography images of PDTBDT-DTFBT/PC$_{71}$BM (a, without DIO, b with 3% DIO) with weight ratio of 1:2.
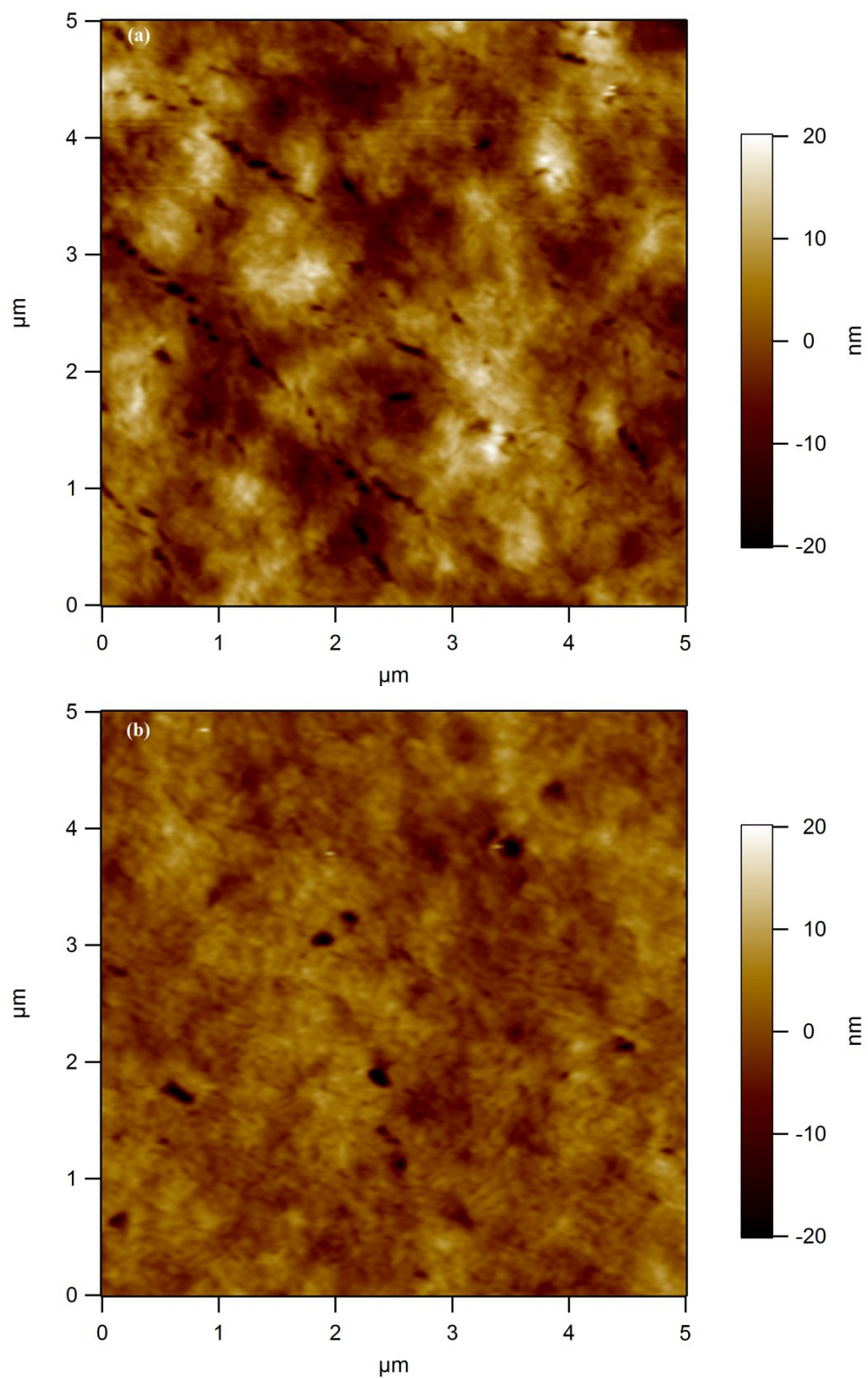

Fig. S17. AFM topography images of PDTBDT-DTFBT/PC$_{71}$BM (a, without DIO, b with 3% DIO) with weight ratio of 1:2.

18. Diagram of the energy levels of the copolymers and PC$_{71}$BM and calculated V$_{oc}$ from empirical equation
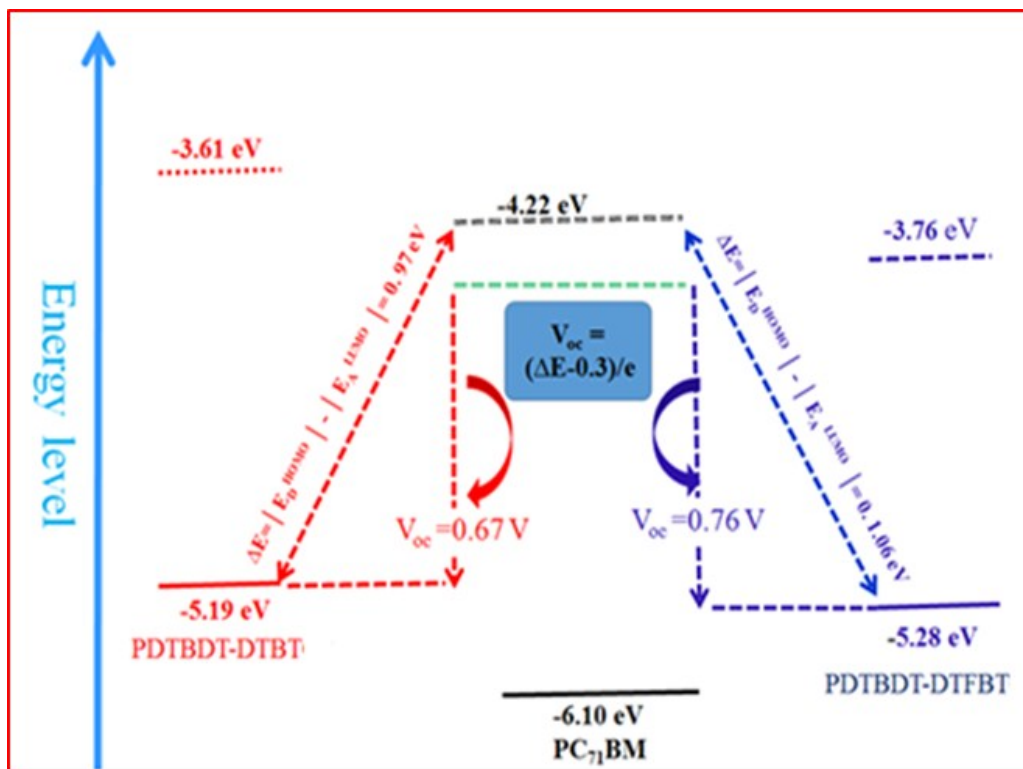

Fig. S18. Diagram of the energy levels of the copolymers and PC$_{71}$BM and calculated *Voc* from empirical equation.